Wave propagation in an elastically supported string with point-wise defects: gap-band and pass-band effects

Evgeny Glushkov[1,*], **Natalia Glushkova**[1], **and Jörg Wauer**[2,**]

[1] Institute for Mathematics, Mechanics and Informatics, Kuban State University, 350040 Krasnodar, Russia
[2] Institut für Technische Mechanik, Universität Karlsruhe, 76128 Karlsruhe, Germany

Wave excitation, propagation and diffraction phenomena as well as related resonance trap-mode, gap-band and pass-band effects occurring in one-dimensional waveguides with obstacles are considered. The waveguide is a spring-supported string with pointwise changed cross-section and/or spring force. The analysis is based on semi-analytical solution in terms of the waveguide's Green functions with unknown coefficients. The latter are obtained from a linear algebraic system whose eigenvalues are spectral points of the problem considered. One of the purposes is to examine the relation between the spectral point allocation in the complex frequency plane and the resonance wave phenomena observed. It is shown that pass-band phenomena are controlled by natural frequencies approaching to the real axis.

1 Introduction

Diffraction of traveling waves in linear waveguides by obstacles leads sometimes to a sharp capture of wave energy which is localized in the form of energy vortices and manifests itself through increased vibration amplitude near the obstacles. This phenomenon is known with different names such as trapped modes in fluid [1, 2], elastic [3] or electromagnetic [4] waveguides, eigenmodes associated with discrete real spectral points of an inhomogeneous elastic strip [5], resonance of inhomogeneous waves in lengthy elastic structures [6], vibration-strength viruses [7], resonant energy vortices [8, 9], and others. Mathematically those effects are connected with the distribution of natural frequencies (resonance poles) ω_n in the complex frequency plane ω: the closer ω_n locates to the real axis, the sounder the resonance effect is.

Those resonance effects are of interest for the development of wave methods for defects location and identification (non-destructive evaluation and structural health monitoring [10, 11]) as well as for the assessment of dynamic strength and failure properties of new laminate composite materials with micro and macro defects. Quite often the resonance diffraction is accompanied by an abrupt screening of incident waves. A sound appearance of the screening effects takes place, in particular, with periodical obstacles, such as systems of interdigital contacts or grooves used in acoustoelectronic frequency filters based on surface acoustic waves [12], or dielectric periodic structures (photonic crystals) with gap bands [13, 14]. Similar band gaps are typical for acoustic wave propagation in periodic composites and crystal structures (atomic phonon lattices) [15–19].

In previous works [8, 9, 20–23] we also considered the trapped-mode, energy localization, pass-band and stop-band effects inherent to elastic layered waveguides with single and multiple obstacles of different kinds (surface slabs, cracks, rigid inclusions, and cavities). The mathematical models used in these investigations have been based on semi-analytical integral representations in terms of Green's matrices of the structures considered. The forms of wave localization are governed here by the eigensolutions $\mathbf{u}_n$ associated with the resonance poles ω_n which are actually the spectral points of integral operators of the related elastodynamic boundary value problems in the frequency domain. In ideally elastic structures certain combinations of obstacles may result in totally real poles ω_n, yielding theoretically interminable undamped oscillation localized near the obstacles. Some examples of eigenforms depicting wave energy localization around one and two cracks in an elastic layer are presented in [9, 22].

It was also found [21] that although the set of resonance poles ω_n for a group of obstacles cannot be obtained as a simple combination of poles corresponding to the individual obstacles taken alone (due to their mutual wave interaction), the blocking properties of the group as a whole is determined in the main by the stop-bands of its individual members.

---

* Corresponding author E-mail: evg@math.kubsu.ru
** E-mail: wauer@itm.uni-karlsruhe.de

Therefore, it turned out to be possible to extend a frequency stop range (gap band) by the use of an aperiodic system of a few obstacles (cracks) with individual spectral points lying close to each other and to the real axis instead of the use of large periodic systems. Further studies of elastic waveguides with multiple defects have shown that inside gap bands there might exist pass frequencies [22, 23]. In the transmission coefficient plots such pass modes appear as narrow peaks centered at frequencies ω_p located closely to the resonance poles ω_n : $\omega_p \approx \mathrm{Re}\,\omega_n$. The number of such pass frequencies ω_p (and correspondingly of the transmission peaks) is proportional to the number of obstacles N but they all are located in a limited frequency range; therefore, as N increases the peaks fill in tightly this range forming a pass band inside a wider gap band.

The main idea of the present study is to get an insight into the mechanism of similar effects in the context of a simpler waveguide model providing a possibility to operate with close analytical representations. Therefore, a spring-supported string with point-wise defects has been chosen as a waveguide. On the one hand, such a structure permits of the trapped mode and wave localization effects [3], on the other hand, its frequency-domain Green function has a simple analytical representation facilitating detailed investigation.

It should be noted that one-dimensional models like strings, rods and beams has also an independent meaning for different engineering applications, e.g. for railway track dynamics simulation [24].

2   Mathematical framework

Let us consider a straight infinite string $-\infty < x < \infty$ lying on a spring foundation (Fig. 1). The dynamic processes in the string are caused by a given incident force $p(x,t)$. The load gives rise to the transverse string displacement $w(x,t)$ that obeys the governing partial differential equation [25]

$$\rho A w_{,tt} + cw - S w_{,xx} = p(x,t) \tag{1}$$

with the homogeneous initial conditions $w(x,0) = w_{,t}(x,0) = 0$. Here ρ is string density, A is its cross-section area, c is spring rate of the foundation, and S is axial pre-stress of the string.
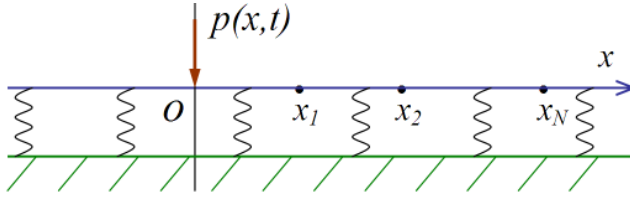

Fig. 1   Springily supported string with defects at points x_j.

It is assumed that this waveguide structure may have a set of defects modeled by the point-wise variation of the spring force c and/or the cross-section mass ρA:

$$c(x) = c_0[1 + \sum_{j=1}^{N} \varepsilon_j \delta(x - x_j)], \quad \rho A(x) = \rho_0 A_0[1 + \sum_{j=1}^{N} \alpha_j \delta(x - x_j)]. \tag{2}$$

Here $\delta(x)$ is Dirac's delta-function, ρ_0, A_0 and c_0 are constant parameters of the homogeneous (free of defects) string, N is a number of defects, x_j are points of defects' location, ε_j and α_j are dimensionless defects' characteristics. Since the constants ε_j control the spring response of the foundation, they specify foundation defects, while α_j determine the point inhomogeneities (defects) of the string itself. With $\alpha_j > 0$ the latter are additional point masses, while negative α_j indicate notch-like or crack defects of the string. With $\alpha_j = -1$ the string cross-section is equal to zero, hence, the lesser values $\alpha_j < -1$ have no physical meaning. Similarly, $\varepsilon_j > 0$ and $\varepsilon_j < 0$ assign respectively greater and lesser spring force than in the homogeneous defect-free base with no any spring response at $x = x_j$ if $\varepsilon_j = -1$. On the whole, the defect constants vary in the limits

$$-1 < \varepsilon_j, \alpha_j < \infty;$$

if $\varepsilon_j = 0$ or $\alpha_j = 0$, there is no any foundation or cross-section defect at the point x_j.

For simplicity, it is assumed that the incident force is a point load applied at the origin:

$$p(x,t) = p_0 \delta(x) f(t) \tag{3}$$

($f(t)$ is a time-shape function of the load), and all of the defects lie on the right of the source: $x_j > 0$.

The transient (time-domain) solution $w(x,t)$ of eq. (1) can be routinely expressed through its frequency spectrum $w(x,\omega)$ using the inverse Fourier transform integral operator $\mathcal{F}_t^{-1}$:

$$w(x,t) = \mathcal{F}_t^{-1}[w(x,\omega)] \equiv \frac{1}{2\pi}\int_{-\infty}^{\infty} w(x,\omega)e^{-i\omega t}d\omega \equiv \frac{1}{\pi}\mathrm{Re}\int_0^{\infty} w(x,\omega)e^{-i\omega t}d\omega. \tag{4}$$

(Hereinafter, when not confusing, we use the same symbols for time-domain functions and their frequency spectra, distinguishing them just by the second argument, e.g. $w(x,t)$ and $w(x,\omega)$.) The spectrum $w(x,\omega)$ obeys the ordinary differential equation

$$Sw_{,xx} + (\omega^2\rho A - c)w = -p_0 F(\omega)\delta(x) \tag{5}$$

which follows from eq. (1) after the application of the forward time-domain Fourier transform

$$\mathcal{F}_t[w(x,t)] \equiv \int_{-\infty}^{\infty} w(x,t)e^{i\omega t}dt = w(x,\omega), \tag{6}$$

assuming that $w(x,t) = w(x,t)_{,t} = 0$ for $t \leq 0$.

In view of the general δ-function property

$$w(x)\delta(x - x_j) = w(x_j)\delta(x - x_j),$$

the δ-constituents in the coefficients of eq. (5) induced by the defects (see eq. (2)) may be replaced by the terms $w_j(\omega^2\rho_0 A_0 \alpha_j - c_0\varepsilon_j)\delta(x - x_j)$ with unknown constant factors $w_j = w(x_j,\omega)$. After transferring those terms into the right-hand side we arrive at the equation

$$Sw_{,xx} + (\omega^2\rho_0 A_0 - c_0)w = -p_0 F(\omega)\delta(x) + \sum_{j=1}^{N} w_j(c_0\varepsilon_j - \omega^2\rho_0 A_0\alpha_j)\delta(x - x_j). \tag{7}$$

To reduce the number of input parameters it is worthy to carry out further calculations in a dimensionless form. The dimensions of constants and variables appearing in eqs. (1) and (7) (in SI units) are

$$[S]=\mathrm{N}=\mathrm{kg}{\cdot}\mathrm{m/s^2}, \qquad [c_0]=\mathrm{N/m^2}=\frac{\mathrm{kg}}{\mathrm{m\,s^2}}, \qquad [t]=\mathrm{s},$$

$$[\rho_0]=\mathrm{kg/m^3}, \qquad [p]=\mathrm{N/m}, \qquad [x]=[x_j]=\mathrm{m},$$

$$[A_0]=\mathrm{m^2}, \qquad [\omega]=\mathrm{radian/s}=\mathrm{rad}{\cdot}\mathrm{Hz}, \qquad [w(x,t)]=\mathrm{m}.$$

We should also take into account that the differentiation and integration change the dimensions: $[w_{,xx}] = [w]/\mathrm{m^2}=1/\mathrm{m}$, $[w_{,tt}] = [w]/\mathrm{s^2}=\mathrm{m/s^2}$, $[w(x,\omega)] = [\mathcal{F}_t w]=\mathrm{m}{\cdot}\mathrm{s}$.

The dimensionless values (indicated by overlines) are introduced as follows

$$\bar{x} = x/h, \quad \bar{x}_j = x_j/h, \quad \bar{w}(\bar{x},\bar{\omega}) = w/(ht_0),$$

$$\bar{\omega} = \omega/f_0 = h\sqrt{\rho_0 A_0/S}\,\omega, \ \bar{c}^2 = h^2 c_0/S \quad (\bar{c}\ \text{is squared for convenience in further calculations}).$$

Here h is a reference length, while $t_0 = h\sqrt{\rho_0 A_0/S}$ and $f_0 = 1/t_0$ are the units of time and frequency. The parameters $\bar{\omega}$ and $\bar{c}^2$ may be referred to as *dimensionless angular frequency* and *relative* (to the string pre-stress S) *base stiffness*, respectively.

Taking into account that

$$S\frac{d^2 w}{dx^2} = \frac{St_0}{h}\frac{d^2\bar{w}}{d\bar{x}^2} = \frac{St_0}{h}\bar{w}''$$

and dividing all the terms of eq. (7) by St_0/h, we arrive at the dimensionless equation

$$\bar{w}'' + k_0^2\bar{w} = -\bar{p}\delta(\bar{x}) + \sum_{j=1}^{N}\bar{w}_j(\bar{c}^2\varepsilon_j - \bar{\omega}^2\alpha_j)\delta(\bar{x} - \bar{x}_j) \tag{8}$$

with

$$k_0^2 = \bar{\omega}^2 - \bar{c}^2 = \frac{h^2 \rho_0 A_0}{S} \omega^2 - \frac{h^2}{S} c_0, \quad \bar{p} = \frac{p_0 F(\omega) h}{S t_0}, \quad \bar{x} = \frac{x}{h}, \quad \bar{w} = \frac{w}{h t_0}.$$

In fact, $\bar{w}(\bar{x}, \bar{\omega})$ is proportional to $\bar{p}$, which enters into the right-hand side of the initial equation as a constant factor. Thus, the independent of load dynamic response of a string with defects (frequency-response characteristic) is introduced as a solution to the equation

$$\bar{w}'' + k_0^2 \bar{w} = \delta(\bar{x}) + \sum_{j=1}^{N} \bar{w}_j (\bar{c}^2 \varepsilon_j - \bar{\omega}^2 \alpha_j) \delta(\bar{x} - \bar{x}_j) \tag{9}$$

which is a special case of eq. (8) with $\bar{p} = -1$. Correspondingly, the dimensional solution (integrand in (4)) is expressed via the dimensionless solution $\bar{w}(\bar{x}, \bar{\omega})$ of eq. (9) in the following way

$$w(x, \omega) = -\bar{p} h t_0 \bar{w}(\bar{x}, \bar{\omega}) = -\frac{h^2}{S} p_0 F(\omega) \bar{w}(x/h, \omega/f_0). \tag{10}$$

Below, the overline above the dimensionless quantities is omitted.

3 Frequency response of defected spring

Just as the diffracted fields excited in 2D and 3D damaged elastic waveguides are favorably to represent in terms of boundary integrals of Green matrix of the defectless structure, it is convenient to express the string frequency response function $w(x, \omega)$ in terms of the Green function $g(x, \omega)$ obeying the equation

$$g'' + k_0^2 g = \delta(x), \quad -\infty < x < \infty. \tag{11}$$

As soon as $g(x)$ is derived, one can write a general solution to eq. (9) in the form

$$w(x, \omega) = g(x, \omega) + \sum_{j=1}^{N} f_j(\omega) g(x - x_j, \omega), \quad f_j = w_j (c^2 \varepsilon_j - \omega^2 \alpha_j), \tag{12}$$

where the only unknowns are the coefficients w_j describing string oscillation at the defected points x_j.

To select the unique fundamental solution, possessing physical meaning from the variety of partial solutions to eq. (11), one has to impose additional constraints on $g(x)$. Conventionally, they are formulated as Sommerfeld radiation conditions and the requirement to be limited at infinity. In that case the fundamental solution, describing harmonic waves excited by the pin-force source applied at the origin $x = 0$, has the form

$$g(x) = \frac{e^{ik_0|x|}}{2ik_0} \tag{13}$$

where with real ω

$$k_0 = \begin{cases} \sqrt{\omega^2 - c^2}, & \omega > c \\ i\sqrt{c^2 - \omega^2}, & |\omega| \le c \\ -\sqrt{\omega^2 - c^2}, & \omega < -c \end{cases}. \tag{14}$$

The first and third of these inequalities provides propagation of undamped harmonic waves $e^{i(k_0|x| - \omega t)}$ from the source to infinity (Sommerfeld radiation condition), while the second one implies zero behavior at infinity ($g \to 0$ as $|x| \to \infty$, $|\omega| < c$). The third condition for $\omega < -c$ is in agreement with the general property of a frequency spectrum

$$g(\tilde{\omega}) = g^*(\omega), \quad \tilde{\omega} = -\omega^*. \tag{15}$$

(Here the asterisk denotes complex conjugation while the tilde marks points which are symmetric in the complex plane with respect to the imaginary axis, e.g. $\tilde{\omega} = -\omega^{(1)} + i\omega^{(2)}$ for $\omega = \omega^{(1)} + i\omega^{(2)}$.) Any harmonic solution (frequency spectrum) $w(\omega)e^{-i\omega t}$ must obey this property to assure the corresponding transient solution $w(t)$ expressed in terms of the inverse Fourier transform (4) to be a real function. Specifically, it assures the identity between the integrals in eq. (4).
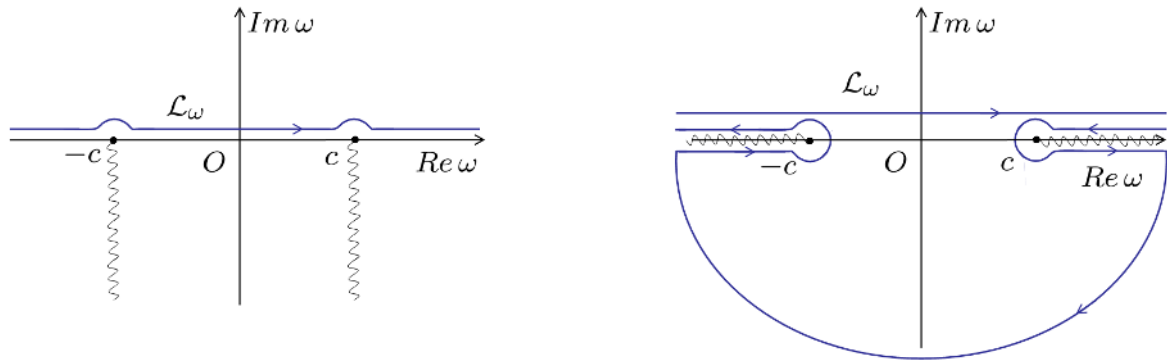
Fig. 2 Integration contour $\mathcal{L}_\omega$ and vertical cuts in the ω-plane (left); horizontal cuts and downward contour closing (right)).

To meet condition (14), it is enough to fix the square-root branches in $k_0 = \sqrt{\omega - c}\sqrt{\omega + c}$ so that $\sqrt{1} = 1$ and the cuts are drawn in the complex ω-plane from the branch points $\pm c$ to infinity beneath the integration contour $\mathcal{L}_\omega$ of the inverse Fourier transform $\mathcal{F}_t^{-1}$ (Fig. 2, left).

The unknown coefficients w_j collected in the vector $\mathbf{w} = [w_1, w_2, ..., w_N]^T$ are obtained then from the linear algebraic system

$$A\mathbf{w} = \mathbf{g} \tag{16}$$

which results from the substitution w of form (12) into the N conditions $w(x_j) = w_j$, $j = 1, 2, ..., N$. The matrix and the right-hand side of this system are

$$A = 2ik_0 I - B, \quad I \text{ is unitary matrix}, \quad B = [b_{ij}]_{i,j=1}^N, \quad b_{ij} = d_j e_{ij},$$

$$d_j = c^2 \varepsilon_j - \omega^2 \alpha_j, \quad e_{ij} = e^{ik_0|x_i - x_j|}, \quad \mathbf{g} = [e_1, e_2, ..., e_N]^T, \quad e_i = e^{ik_0|x_i|}.$$

Natural frequencies ω_n of the defected string coincide with the roots of the characteristic equation

$$\Delta(\omega) \equiv \det A(\omega) = 0, \tag{17}$$

where A is the matrix of system (16). The eigensolutions $w_n(x)$ associated with the eigenfrequencies ω_n are of form (12) with w_j to be the elements of eigenvectors $\mathbf{w}_n : A(\omega_n)\mathbf{w}_n = 0$.

Remark 1 The technique above based on expansion in terms of fundamental solution $g(x)$ derived for an infinite string is quite applicable in the case of a finite string as well. For example, if a finite string $-a \le x \le a$ is fixed at the ends: $w(\pm a) = 0$, then it is enough to introduce two extra terms $s^- g(x + a)$ and $s^+ g(x - a)$ into expression (12), substituting it into the $N + 2$ conditions at the points x_j and $\pm a$, to reduce the problem to a linear algebraic system with respect to the vector $\mathbf{w} = [s^-, w_1, w_2, ..., w_N, s^+]^T$.

4 Time-domain analysis

4.1 Free of defects string

Transient propagation of a pulse $w(x, t)$ excited in a defectless string by a given load (3) is described by integrals (4) with $w(x, \omega) = g(x, \omega)F(\omega)$ taken over a contour $\mathcal{L}_\omega$, which deviates upward from the real axis going around the integrand's singular points. If $f(t) = \delta(t)$, the pulse spectrum $F(\omega) = 1$ and the solution

$$w(x, t) = \mathcal{F}_t^{-1}[g(x, \omega)] = g(x, t)$$

is nothing but the transient Green function of the homogeneous waveguide. With an arbitrary $f(t)$ the time-domain solution may be written as the convolution of g with f:

$$w(x,t) = g * f = \int\limits_0^\infty g(x, t - \tau) f(\tau) d\tau.$$

Thus the waveguide properties are specified by $g(x,t)$ and its frequency spectrum $g(x,\omega)$ of form (13). In the range $c < \omega < \infty$ the wave number k_0 is real and the function $g(x,\omega)$ represents undamped harmonic traveling waves propagating to infinity with phase velocity $v_p = \omega/k_0$ and group velocity $v_g = d\omega/dk_0 = k_0/\omega = 1/v_p$. Since they depend on frequency, the propagation is dispersive with the dimensionless v_p descending from infinity to unity and v_g increasing from zero to unity as ω varies from the cut-off frequency $\omega = c$ to infinity (Fig. 3). In the range $0 \leq \omega < c$ the wave number k_0 is complex and the related oscillations are exponentially decaying as $|x| \to \infty$, i.e. the waveguide is locked.

The frequency spectrum $w = g(x,\omega)$ exhibits sharp infinite growth at $\omega = c$ (Fig. 4), however, this point is not a pole, but a weak (square-root) singularity and a branch point of the solution. Consequently, the continuous spectrum of the defectless problem, yielding traveling waves, coincides with the semi-infinite real-axis segments $c \leq |\mathrm{Re}\,\omega| < \infty$, $\mathrm{Im}\,\omega = 0$ with no discrete spectral points in the ω-plane.
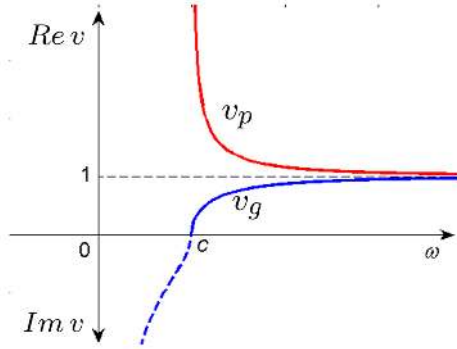

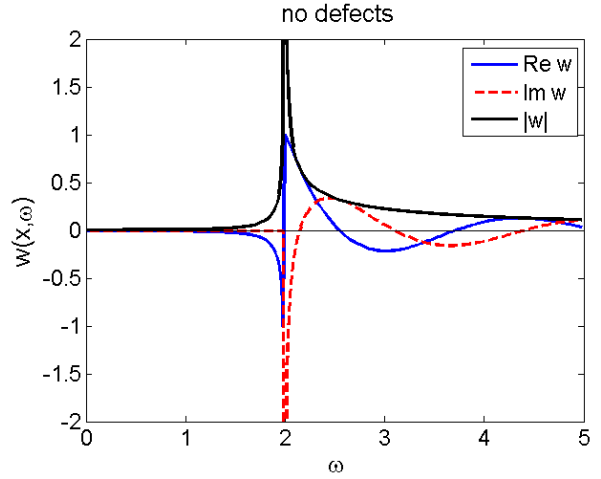**Fig. 3** Phase and group velocities for a defect-free string.

Fig. 4 Frequency spectrum $w = g(x,\omega)$ of a defectless string; $c = 2$, $x = 2$.

The transient Green function $g(x,t)$ may be expressed as an integral superposition of propagating waves over the continuous spectrum. For that it is enough to draw the cuts starting from the branch points $\pm c$ along the real axis but beneath the integration contour $\mathcal{L}_\omega$ (Fig. 2, right) and to close it basing on the Jordan lemma.

By the analysis of radicals (14) extended analytically into the upper half-plane $\mathrm{Im}\,\omega > 0$ it can be shown that

$$k_0(\omega) \sim \omega, \quad \text{and} \quad e^{ik_0|x|} e^{-i\omega t} \sim e^{i\omega(|x|-t)}, \quad \text{as} \quad |\omega| \to \infty, \ \mathrm{Im}\,\omega > 0.$$

Hence, with any $|x| - t > 0$

$$g(x,\omega) e^{-i\omega t} \to 0, \quad \text{as} \quad |\omega| \to \infty, \ \mathrm{Im}\,\omega > 0,$$

and the integration contour $\mathcal{L}_\omega$ can be closed into the upper half-plane $\mathrm{Im}\,\omega > 0$ without any poles inside. In accordance with the Cauchy theorem it implies the quiescent state

$$g(x,t) \equiv 0 \quad \text{for} \quad 0 \leq t < |x|. \tag{18}$$

That is, in spite of the fact that for all ω the phase velocities of harmonic constituents $v_p > 1$, the leading edge of the Green function pulse comes to an observation point with the limiting group velocity $\sup v_g = 1$.

As $t > |x|$, the contour can be closed downward, rounding the cuts along their sides (Fig. 2, right). Since there are no any other singularities (poles) in the complex plane ω in this case, the path integral (4) is equal to the minus integrals along

the cut sides $[\pm c, \pm\infty]$ or, finally, it may be reduced to the form

$$
\begin{aligned}
w(x,t) \quad &= \frac{1}{2\pi} \int_{\mathcal{L}_\omega} g(x,\omega)e^{-i\omega t}d\omega = \frac{2}{\pi}\int_c^\infty \operatorname{Im} g(x,\omega)\sin\omega t d\omega = \\
&= -\frac{1}{\pi}\int_c^\infty \frac{\cos k_0|x|}{k_0}\sin\omega t d\omega, \quad t > |x|
\end{aligned}
\tag{19}
$$

where $k_0 = \sqrt{\omega^2 - c^2} > 0$ is the value of k_0 at the upper bank of the cut $c < \omega < \infty$.

Remark 2 Whereas eq. (19) demonstrates how the continuous spectrum contributes into the wave structure, the vertical cuts (Fig. 2, left) are more preferable for numerical integration because the integrands decrease exponentially as $\operatorname{Im}\omega \to -\infty$ along such cuts. Henceforth, we fix such cuts for the numerical examples below.

4.2 Defected string

Expansion (12) can be interpreted as a superposition of complex amplitudes of time-harmonic waves excited by the original point source $p = \delta(x)\delta(t)$ (the first term g) and diffracted by the defects (all other terms $f_j g(x - x_j)$). The defects act here as the point sources $p = \delta(x - x_j)f_j(t)$ with the frequency spectra $f_j(\omega)$ of their time-shape functions given by the expansion coefficients (12). The latter are proportional to the defect vibration amplitudes $w_j(\omega)$ and are controlled in addition by the defect parameters ε_j and α_j via the factors $d_j = c^2\varepsilon_j - \omega^2\alpha_j$.

The transform $\mathcal{F}_t^{-1}$ converts eq. (12) into the time-domain, yielding the transient string response in terms of the incident pulse $g(x,t)$ and re-excited by defects pulses $u_j(x,t)$:

$$
\begin{aligned}
&w(x,t) = g(x,t) + \sum_{j=1}^N u_j(x,t), \\
&u_j(x,t) = f_j * g_j \equiv \int_{|x-x_j|}^{t-x_j} f_j(t-\tau)g(x-x_j,\tau)d\tau.
\end{aligned}
\tag{20}
$$

Obviously,

$$
u_j(x,t) \equiv 0 \quad \text{if} \quad t < x_j + |x - x_j|,
\tag{21}
$$

i.e., if the upper limit of integration is less than the lower one.

The bottom limit of the convolution integral follows from the fact that $g(x - x_j, \tau) \equiv 0$ for $\tau < |x - x_j|$ (see eq. (18)). It means, no signals come to the observation point x from the defect point x_j earlier than the rise-up portion going with the unit velocity.

The upper limit is also determined by a quiescent period but, for this once, of the pulse-shape function: $f_j(t) \equiv 0$ for $t < x_j$, entailing $f_j(t - \tau) \equiv 0$ if $\tau > t - x_j$. This is in agreement with the physical consideration showing that the defect must be in rest up to the time $t = x_j$ when the wavefront coming from the origin turns it on. Mathematically the rest period $t < x_j$ follows from the main exponential behavior

$$
f_j(\omega) \sim O(e^{i\omega x_j}), \quad \operatorname{Im}\omega \to \infty
\tag{22}
$$

of its frequency spectrum in the upper half-plane of the complex ω-plane, which is conditioned by the elements $e_j = e^{ik_0|x_j|}$ of the right-hand side $\mathbf{g}$ of system (16). Such behavior allows one to close the integration contour $\mathcal{L}_\omega$ in the representation

$$
f_j(t) = \mathcal{F}_t^{-1}[f_j(\omega)] \equiv \frac{1}{2\pi}\int_{\mathcal{L}_\omega} f_j(\omega)e^{-i\omega t}d\omega
\tag{23}
$$

upward for $x_j - t > 0$, getting $f_j(t) \equiv 0$ due to the absence of singularities in the upper half-plane.

The diffracted pulses u_j may also be expressed via their frequency spectra

$$
u_j(x,t) = \frac{1}{2\pi}\int_{\mathcal{L}_\omega} f_j(\omega)g(x-x_j,\omega)e^{-i\omega t}d\omega.
\tag{24}
$$

As above, $\mathcal{L}_\omega$ can be closed upward for $t < x_j + |x - x_j|$ resulting in the quiescent property (21). The limiting time $t = x_j + |x - x_j|$ is required for coming with the unit velocity from the origin to the defect ($t = x_j$) and then from the turned-on defect source $f_j(t)\delta(x - x_j)$ to a point of observation x ($t = |x - x_j|$).

The downward closing with $t > x_j + |x - x_j|$ leads, the same way as in eq. (19), to the integration along the cuts plus the contribution of residuals from the resonance poles ω_n. In other words, this yields a sum of the continuous and discrete spectrum contributions into the total wave field. General property (15) implies that every complex pole ω_n: $\operatorname{Re}\omega_n > 0$, must have its symmetric counterpart $\tilde{\omega}_n$. Therefore, from now on only the right poles ($\operatorname{Re}\omega_n > 0$) are denoted as ω_n, while the left ones are $\tilde{\omega}_n$ or $-\omega_n$ for real poles. The residuals from such pole pairs of a frequency spectrum function $u(\omega)$ extended analytically into the lower complex half-plane are also symmetric with respect to the imaginary axis:

$$r_n = \operatorname{res} u(\omega)|_{\omega=\omega_n} \quad \Rightarrow \quad \operatorname{res} u(\omega)|_{\omega=\tilde{\omega}_n} = \tilde{r}_n.$$

Consequently, the pair of residuals from ω_n and $\tilde{\omega}_n$ yields a real transient signal

$$u_n(x,t) = -\frac{2\pi i}{2\pi}(r_n e^{-i\omega_n t} + \tilde{r}_n e^{-i\tilde{\omega}_n t}) = 2\operatorname{Im}[r_n(x)e^{-i\omega_n t}]. \tag{25}$$

As is well-known, if ω_n is a real pole, $u_n(x,t)$ describes undamped harmonic oscillation at every fixed point x, while a complex pole lying in the lower half-plane ($\operatorname{Im}\omega_n < 0$) results in an exponentially decaying harmonics with the logarithmic decrement $\delta_n = |\operatorname{Im}\omega_n|$: $u_n(t) \sim O(e^{-\delta_n t})$ as $t \to \infty$. The trapped mode effect takes place with real and nearly real spectral points ω_n.

If ω_n lies in the stop range $0 < \omega < c$, the undamped oscillation $u_n(x,t)$ is spatially localized near defects. Indeed, the wave number $k_0(\omega_n) = i\sqrt{c^2 - \omega_n^2}$ is purely imaginary at this point, and the residuals from the main exponential parts (22) of the coefficients of sum (12) contribute in the amplitude $r_n(x)$ as $\sum_j r_{jn}$, where $|r_{jn}| = a_j e^{-|k_0|(x_j + |x - x_j|)}$, $a_j = \text{const}$. Hence the amplitude of those terms are maximal at the points of defect location x_j, decreasing exponentially as $O(e^{-|k_0||x - x_j|})$ with the increasing distance from the defect $|x - x_j|$. The factors $e^{-|k_0|x_j}$ show that due to non-propagating character of vibration at $\omega = \omega_n < c$ the maximum of the localized oscillation also decreases exponentially with the defect's distance x_j from the source located at $x = 0$. Thus, although the real spectral points $\omega_n < c$ result in interminable oscillation, its amplitude decays exponentially with the distance from both the source and the defects.

With $\omega_n > c$ the wave number $k_0(\omega_n) = \sqrt{\omega_n^2 - c^2}$ is real and the residuals would give undamped propagating waves. However, in the problem considered no real poles ω_n have been found in this range $\omega > c$. Their absence with any defect parameters α_j and ε_j can be easily proved for the cases of one and two defects, while for $N \geq 3$ it can be strictly checked for any fixed α_j and ε_j by analyzing the root location of the characteristic equation (17). Nevertheless, with certain defect parameters nearly real poles ω_n: $\operatorname{Re}\omega_n > c$, $\operatorname{Im}\omega_n < 0$, $|\operatorname{Im}\omega_n|/\operatorname{Re}\omega_n << 1$ occur in the lower half-plane. In more detail the pole location is analyzed in the next section.

5 Spectral analysis

5.1 One defect

With $N = 1$ system (16) is a scalar equation which yields

$$w_1 = \frac{g_1}{2ik_0 - b_{11}} = \frac{e^{ik_0 x_1}}{\Delta(\omega)}, \quad \Delta(\omega) = 2ik_0 - c^2\varepsilon + \omega^2\alpha \quad (\varepsilon = \varepsilon_1, \ \alpha = \alpha_1). \tag{26}$$

On the whole (see eq. (12))

$$w(x,\omega) = \frac{1}{2ik_0}\left[e^{ik_0|x|} + \frac{c^2\varepsilon - \omega^2\alpha}{\Delta(\omega)}e^{ik_0(x_1 + |x - x_1|)}\right]. \tag{27}$$

It is easily seen that the expression in brackets tends to zero as $k_0 \to 0$ (if $\varepsilon \neq \alpha$). It means, the weak singularity $\omega = c$ is eliminable and other singularities can only be induced by the roots of the characteristic equation $\Delta(\omega) = 0$. With $\varepsilon = \alpha$ the square-root singularity is non-eliminable.

The characteristic equation cannot have any real root if k_0 is real, i.e. in the range $\omega^2 > c^2$. It follows from the fact that with real k_0 the first term $2ik_0$ is pure imaginary, while the rest part is real. On the contrary, $\Delta(\omega)$ is totally real in the band $\omega^2 < c^2$, so it may have real roots there.

For $\alpha > 0$ the only real pole

$$\omega_1 = \sqrt{\alpha\varepsilon c^2 - 2 + 2\sqrt{1 + \alpha c^2(\alpha - \varepsilon)}}/\alpha.$$

exists if the input parameters meet the limitation $\max\left[-2/c; -1\right] < \varepsilon < \alpha < \infty$.

With $\alpha = 0$ (no mass defect),

$$\omega_1 = c\sqrt{1 - \varepsilon^2 c^2/4}, \quad |\varepsilon|c < 2.$$

With $\alpha < 0$ no real roots are possible if $\varepsilon > \alpha$ (as above), while with $\varepsilon < \alpha < 0$ two real poles

$$\omega_{1,2} = \sqrt{\alpha\varepsilon c^2 - 2 \pm 2\sqrt{1 + \alpha c^2(\alpha - \varepsilon)}}/\alpha$$

occur if both radicands are positive: $|\alpha|c^2 < 1/(|\varepsilon| - |\alpha|), \quad \alpha, \varepsilon < 0, \ |\varepsilon| > |\alpha|$ and $(\alpha\varepsilon c^2 - 2)^2 > 4(1 + \alpha c^2(\alpha - \varepsilon)) \Rightarrow |\varepsilon|c > 2$.

Examples of real-pole curves $\omega_n(\varepsilon)$ with fixed α are given in Fig. 5 for the spring force $c = 2$ (left) and $c = 4$ (right). The two-pole situation takes place, for example, with $c = 4$, $\alpha = -0.5$, $\varepsilon < \alpha = -2/c$. Examples of frequency spectra in the one-pole and two-pole cases are depicted in Fig. 6. Thus, the real positive pole $\omega_1 < c$ almost always exists if $\varepsilon < \alpha$. If ε becomes greater than α it leaves the real axis passing the point $\omega = c$ as $\varepsilon = \alpha$. At this point the pole is eliminable, but the weak singularity $(\omega^2 - c^2)^{-1/2}$ becomes apparent instead. Obviously, no other poles ω_n may exist in the one-defect case.
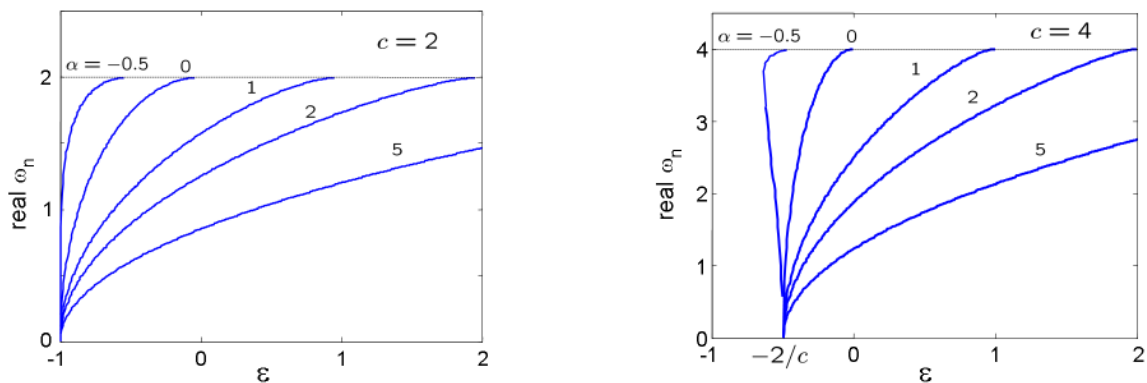

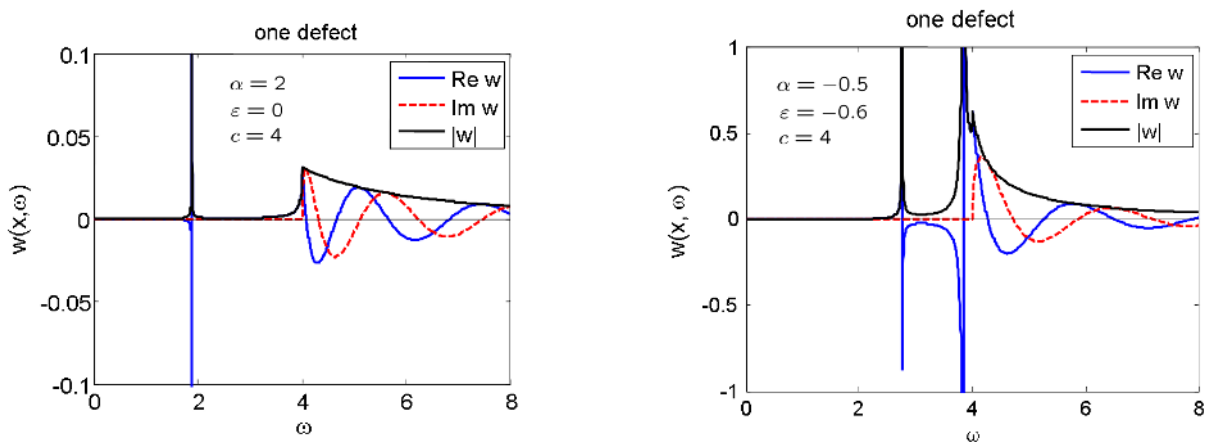
Fig. 5 Real poles in the one-defect case.

Fig. 6 Harmonic spectrum $w(x, \omega)$ at the point of defect location $x = x_1 = 2$; one real pole (left) and two real poles (right).

5.2 Two and more defects

With $N = 2$ the matrix of system (16) takes the form

$$A = \begin{pmatrix} 2ik_0 - d_1 & -d_2 e \\ -d_1 e & 2ik_0 - d_2 \end{pmatrix}, \quad d_j = c^2 \varepsilon_j - \omega^2 \alpha_j, \quad e = e^{ik_0 a}, \quad a = |x_2 - x_1|.$$

Hence, the determinant $\Delta = \det A$ can also be written in a closed form:

$$\Delta = (2ik_0 - d_1)(2ik_0 - d_2) - d_1 d_2 e^2 = 0.$$

With $\omega < c$ this function $\Delta(\omega)$ is pure real and may have real roots. Examples of root plots for two equal defects ($\alpha_1 = \alpha_2 = \alpha$, $\varepsilon_1 = \varepsilon_2 = \varepsilon$) with the spacing $a = 1, 0.5, 0.2$ and 0.1 are given in Fig. 7. One can see that two obstacles
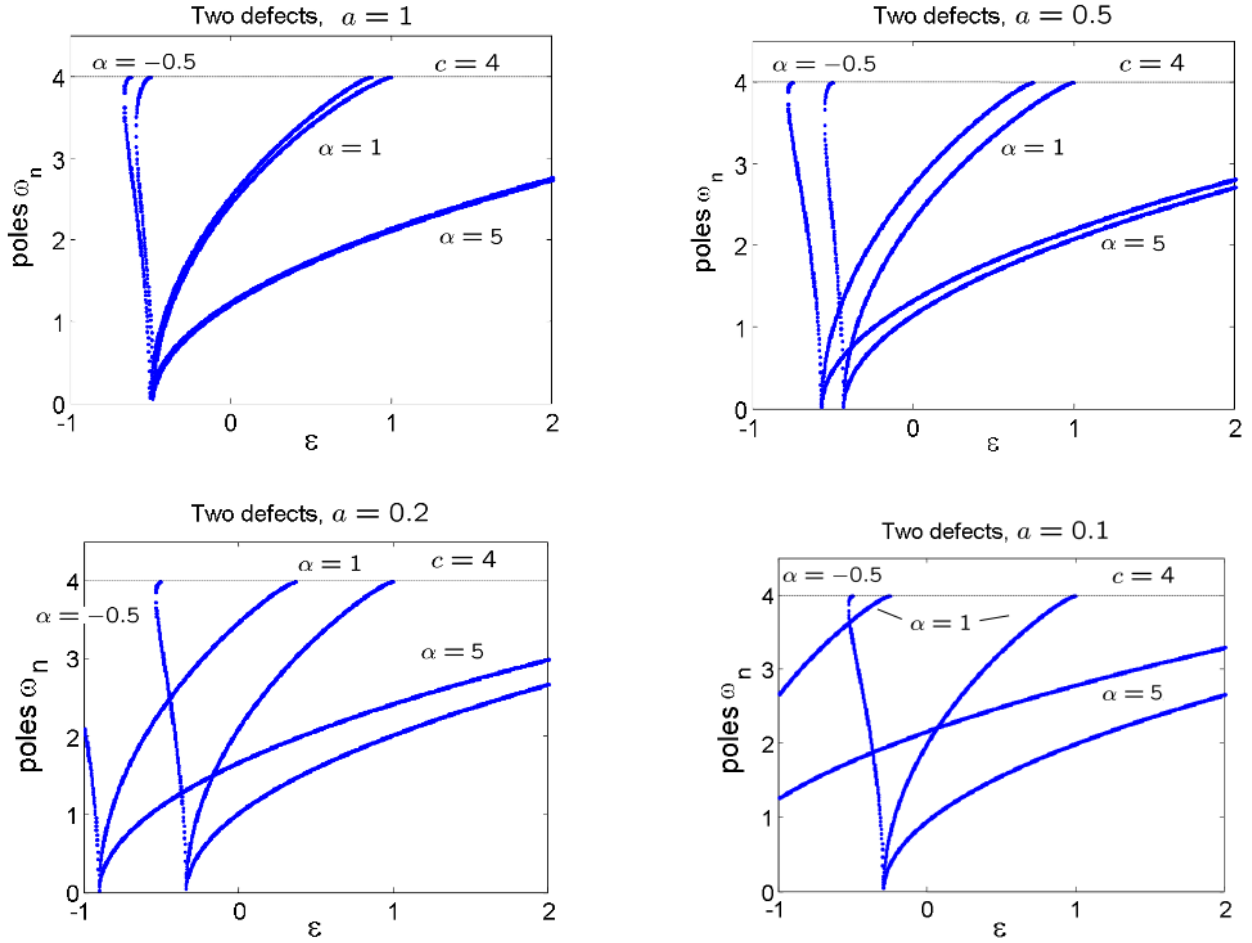
Fig. 7 Real poles ω_n for strings with two equal defects spaced the distance $a = 1, 0.5, 0.2$ and 0.1 apart.

result in two bush-form families of polar curves branching off from the two exit points $\varepsilon = \varepsilon_1^*$ and $\varepsilon = \varepsilon_2^*$ at the left and at the right of the point $\varepsilon^* = -2/c = -0.5$ ($\varepsilon_1^* < \varepsilon^* < \varepsilon_2^*$). The latter is the exit point of the only bush family inherent to the one-defect case shown in Fig. 5. The number of such polar curves increases in parallel with the number of obstacles (Fig. 8). With a large a (e.g. $a = 1$ in the first subplot of Fig. 7), those exit points ε_1^* and ε_2^* are very close to each other and to ε^*, so that with any fixed α two emanating polar curves go almost together following the one-defect trajectory. It reflects the fact that the mutual wave interaction of distant defects become weak and they oscillate as independent obstacles with practically the same resonance properties as with the one-defect string.

As the distance a shrinks, the exit points and the polar curves move apart, the right bush is more conservative remaining not far from the one-defect polar curves, while the left polar bush accelerates as $a \to 0$, leaving completely the admissible range $\varepsilon > -1$ with $a < 0.02$.

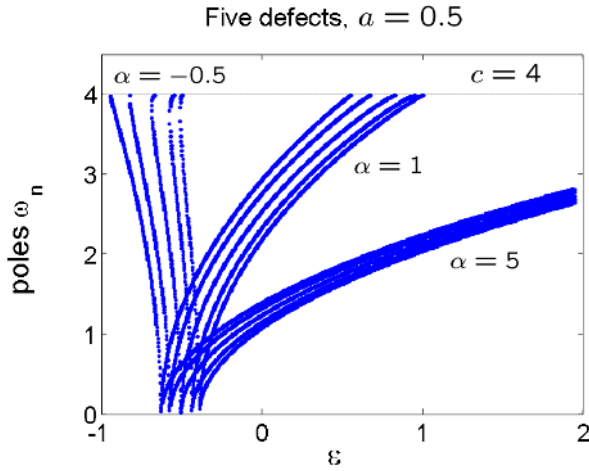**Fig. 8** Real poles ω_n for five-defect strings, even spacing $a = 0.5$.

On the continuous spectrum $\omega > c$ the characteristic equation $\Delta(\omega)$ is complex and its real and imaginary parts must be equated to zero simultaneously:

$$\begin{cases} \cos 2k_0 a = 1 - 4k_0^2/(d_1 d_2) \\ \sin 2k_0 a = -2k_0(d_1 + d_2)/(d_1 d_2). \end{cases} \tag{28}$$

The squaring of both lines of this system and their subsequent adding leads to the equation

$$d_1^2 + d_2^2 + 4k_0^2 = 0$$

which, obviously, cannot have real roots to be a sum of positive terms (squares). Hence, no real resonance frequencies are possible in the traveling wave range $\omega > c$, similarly to the single-defect case above.

5.3   Nearly real poles

The presence of the exponential factors $e_{ij} = e^{ik_0|x_i - x_j|}$ in the matrix of system (16), which are infinitely periodic functions ($e^{i(z+2\pi n)} = e^{iz}$), hints at the infinite number of roots ω_n as $N \geq 2$. These roots should be allocated more or less periodically in the complex ω-plane. Indeed, the search for nearly real complex ω_n has revealed such groups of poles adjacent to the real axis from below ($\operatorname{Im} \omega_n < 0$) and located quasi-periodically along the axis (Fig. 9 - 10).

These figures give examples of ω_n location in the case of N evenly spaced defects ($a = 1$) with parameters $\alpha = 0.5$, $\varepsilon = 0.5$ (Fig. 9) and $\alpha = 0$, $\varepsilon = 1$ (Fig. 10). The parameters are chosen to illustrate two quantitatively different patterns of pole locations as N increases: shrinking into small groups (Fig. 9) or spreading along the real axis (Fig. 10) as $\omega \to \infty$. The latter occurs only with $\alpha = 0$, i.e. when the string itself is defectless and the obstacles can only be in the spring base ($\varepsilon \neq 0$). In such a case the transmission coefficient tends to unit as $\omega \to \infty$, i.e. the base inhomogeneities cease to shield the wave propagation at high frequencies if the string itself is intact (e.g. see the dashed lines for $N = 1$ in Fig. 16 below). On the contrary, with any string defects, both with additional masses ($\alpha > 0$) and notch-like cracks ($\alpha < 0$), the wave propagation at high frequencies becomes fully blocked (e.g. Figs. 11 – 13).

The circle markers in Figs. 9 – 10 point out the location of complex natural frequencies of two-defected strings. It is seen that in both cases they go along the real axis with the period $\operatorname{Re} \omega_{n+1} - \operatorname{Re} \omega_n \approx \pi$, rising up to the axis as $\operatorname{Re} \omega_n$ increases in the first case (Fig. 9) and, contrariwise, going down in the second example (Fig. 10). The groups of $N - 1$ poles appear above these marked by circles places as N becomes greater than two, moving up closely to the real axis as $N \to \infty$ in both cases. The right subplots of both figures are enlarged fragments demonstrating the patterns of pole groups with large N. In both cases they are arranged along arched-down curves that are pulled up to the axis as $N \to \infty$. In the first case (Fig. 9, left) the frequency bands (segments of the real axis) to which the pole groups approach are separated by increasing intervals so that these bands shrink in points as $\omega \to \infty$. Quite the contrary, such bands increase and the intervals between them shrink as $\omega \to \infty$ in the second case (Fig. 10, left). These rules of the nearly real complex pole distribution play the key role in the resonance gap-band and pass-band occurrences considered in the next section.
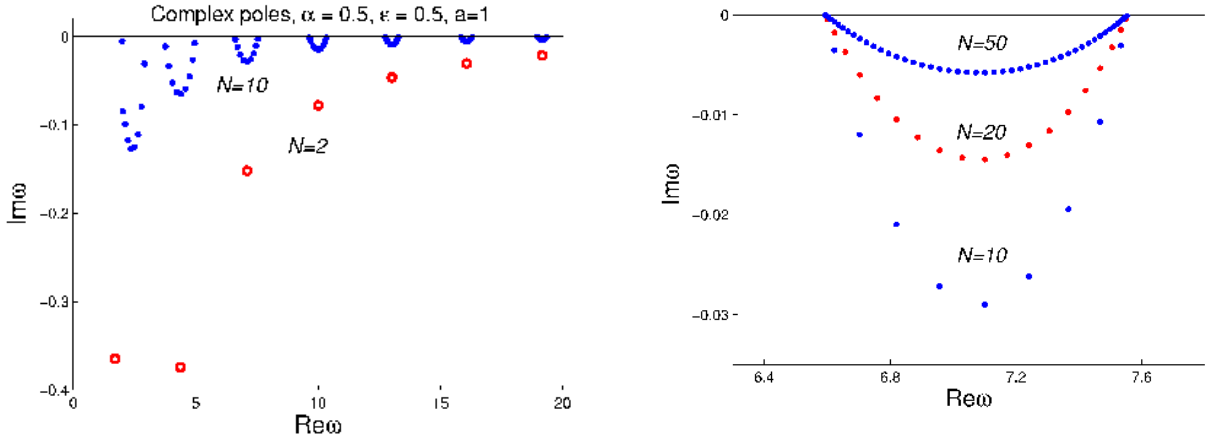
Fig. 9 Nearly real pole allocation in the complex ω-plane for N evenly spaced defects ($\alpha = \varepsilon = 0.5$, $a = 1$).
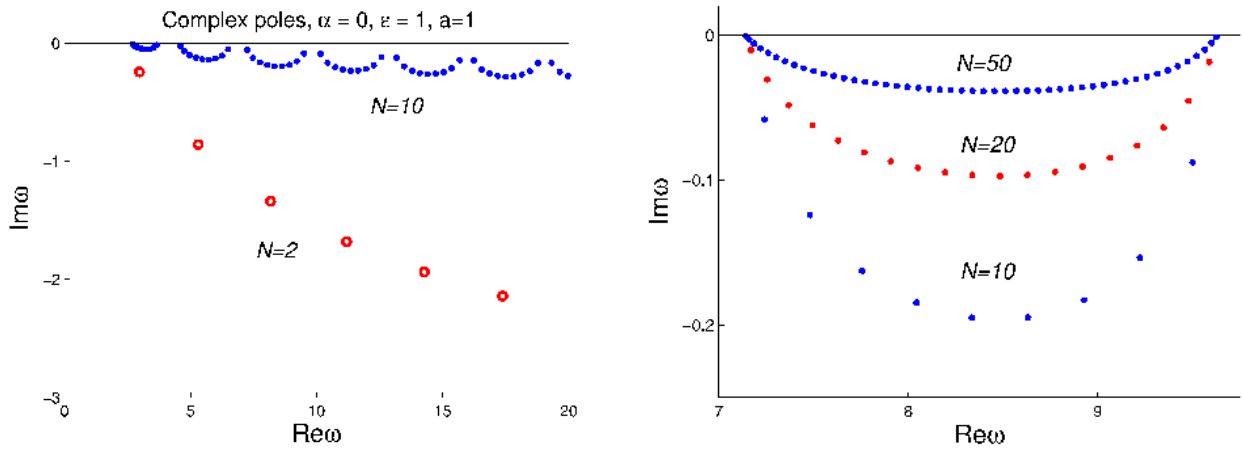

Fig. 10 The same as in Fig. 9 but for spring defects ($\alpha = 0$, $\varepsilon = 1$, $a = 1$).

6   Wave transmission through the defected zone

Let us introduce the wave-transmission coefficient κ^+ as the ratio

$$\kappa^+ = |w(x^+, \omega)|^2/|g(x^+, \omega)|^2, \quad \omega > c \tag{29}$$

where $x^+ > x_N$ is any point on the right of defects. This ratio shows how much the squared amplitude of string oscillation behind the defects becomes less than the oscillation of the defect-free string. Since the factor $e^{ik_0 x}$ can be brought out and canceled, κ^+ is independent of a specific location of the receiving point x^+. Normally κ^+ varies in the range $0 \leq \kappa^+ \leq 1$; $\kappa^+ = 0$ indicates the full stopping of wave propagation by the defects, while $\kappa^+ = 1$ means that the defects are quasi-transparent not telling on the wave transmission (full-passing mode).

6.1   Transmission by single defects

For a single defect $\kappa^+ = 4k_0^2/|2ik_0 - c^2\varepsilon + \omega^2\alpha|^2$. Figs. 11−13 depicting κ^+ versus ω give an idea of single-defect screening properties.   solitary obstacles. The left subplot of Fig. 11 is for strings with a damaged cross-section ($\alpha_1 = \alpha \neq 0$) and an intact spring foundation ($\varepsilon_1 = \varepsilon = 0$, $c = 2$; this value c is kept on default in all numerical examples of this section). One can see that the defect's shielding ability increases as $|\alpha|$ grows up; it is the same for negative and positive α
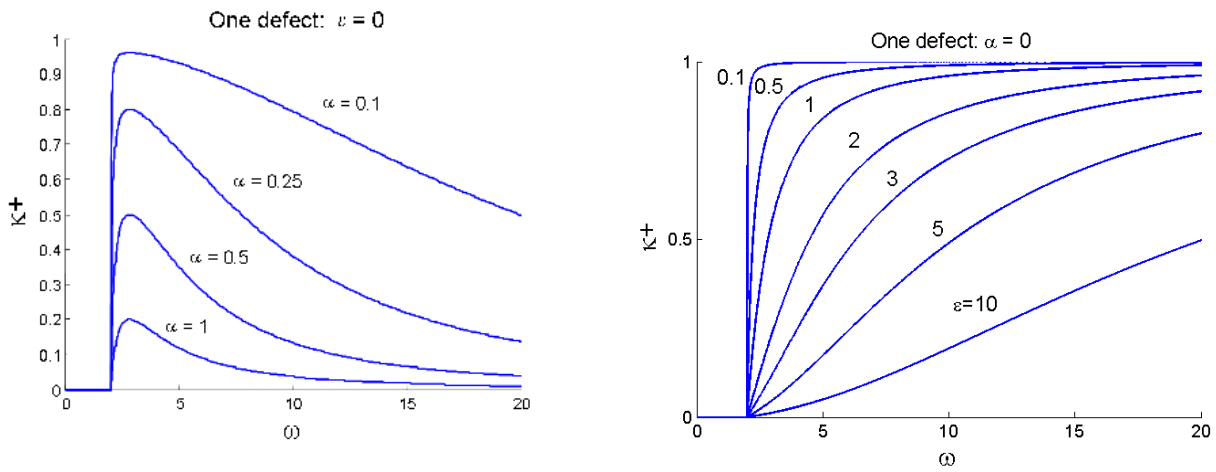
Fig. 11 Screening properties of a single string defect ($\varepsilon = 0$, $\alpha \neq 0$, left) and base defect ($\varepsilon \neq 0$, $\alpha = 0$, right).
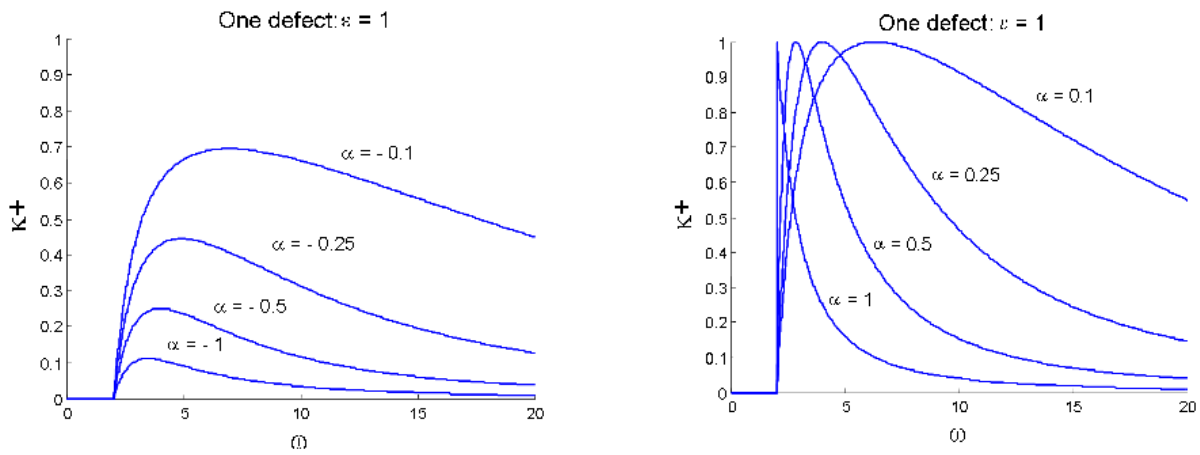

Fig. 12 The same as in Fig. 11 for a single combined obstacle with the fixed base damage $\varepsilon = 1$ and different string inhomogeneities $\alpha < 0$ (left) and $\alpha > 0$ (right).
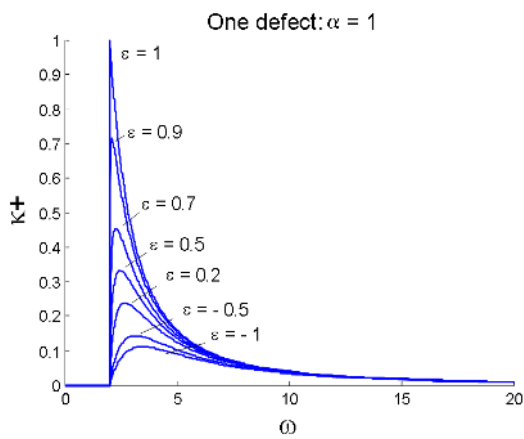

Fig. 13 Shielding property of a single defect with $\varepsilon \leq \alpha$.

of equal absolute value. The right subplot of Fig. 11 illustrates the one-defect screening in the case of intact string ($\alpha = 0$) and defected foundation ($\varepsilon \neq 0$). It also depends only on the absolute value $|\varepsilon|$.

On the contrary, a combined obstacle does not possesses such a symmetry (e.g., Fig. 12 for $\varepsilon = 1$). With $\alpha > 0$ (right subplot) every curve $\kappa^+(\omega)$ reaches the maximal value $\kappa^+ = 1$ at an isolated specific frequency $\omega = \omega_p$, which is the lower the larger α is. At this frequency ω_p the defect becomes invisible for an incident harmonic wave. Such pass frequencies take place if $\varepsilon \geq \alpha > 0$. With $\varepsilon < \alpha \ \max \kappa^+(\omega) < 1$ decreasing monotonously as ε goes down and α is fixed (Fig. 13).

6.2   Resonance passing and blocking with multiple periodic defects

The character of wave transmission through a zone with several equal defects is essentially different to that in the one-defect case. The $\kappa^+(\omega)$ plots are featured by periodic peaks reaching $\kappa^+ = 1$ and alternating with deep depressions (gap bands). The peak spacing for a two-defect string depends merely on the distance between the obstacles $a = |x_2 - x_1|$, to be inversely proportional to this value a (see Fig. 14 for two notch-like defects and intact base: $\alpha = -0.5$, $\varepsilon = 0$; hereinafter the dashed line is $\kappa^+(\omega)$ for the corresponding one-defect string).

The period of alternation of peak zones (pass bands) keeps to be the same with any number of equal defects spaced the same distance $|x_{j+1} - x_j| = a$, $j = 1, 2, ..., N - 1$ apart (Fig. 15 for N defects $\alpha = \varepsilon = 0.5$, $a = 1$; the same as in the complex poles examples given in Fig. 9). Each of the peaks is composed of $N - 1$ narrow sub-peaks located in the frequency ranges of the approximately same band widths regardless of the number of defects N. Needless to say that the peaks are centered above the complex poles ω_n shown in Fig. 9. With increasing N those sub-peaks flood in the pass bands completely. Since all of them reach the highest level $\kappa^+ = 1$, the plots above the pass bands look like tops of painted rectangles limited from below by white arches. The arches' tops touch the dashed line for the one-defect $\kappa^+(\omega)$. In accordance with the pole behavior the width of pass bands decreases with increasing frequency ω down to the degeneration into discrete pass-frequencies at infinity.

Multiple periodic defects in the elastic base with intact string (the same as in Fig. 10) also lead to the development of pass and gap bands as N increases (Fig. 16). The main difference to the previous case of damaged strings ($\alpha \neq 0$) is that with increasing ω a sole defect lets more and more part of wave energy to pass by (dashed curve). Conformably to the poles allocation, the gap bands shrink with increasing ω instead of pass bands, so that almost no breaks for wave propagation occur at high frequencies. As N increases, the poles also nestle up to the real axis and the downward excursions (dips) of $\kappa^+(\omega)$ become deeper and deeper, practically touching zero level with $N = 20$.

Thus, we have ascertained once again that resonance peaks of frequency characteristics indicate the presence of complex poles ω_n located very close to the real axis. Earlier this fact was observed for a 2D elastic strip waveguide with horizontal cracks or inclusions as defects [22, 23]. Whereas the nearly real natural resonance frequencies ω_n of a solitary crack resulted in sharp narrow gaps in the $\kappa^+(\omega)$ plots [9], narrow pass peaks appeared inside the gap band just at the resonance frequencies $\omega \approx \operatorname{Re} \omega_n$ with two [22] and more [23] obstacles. The number of such sub-peaks (and so the poles ω_n) in each pass-band group was $N - 1$, just the same as in the present string examples where the resonance pass effect also occurs at $\omega \approx \operatorname{Re} \omega_n$. Taking into account that the location of pass bands on the frequency axis remains practically the same with any N down to $N = 2$, we may estimate their localization analytically by analyzing the simplest characteristic equation (28) for two defects. It is easily seen that

$$\begin{cases} \cos 2k_0 a = 1 + O(\omega^{-2}) \\ \sin 2k_0 a = O(\omega^{-1}) \end{cases}, \quad \text{as} \quad \omega \to \infty.$$

It means

$$2k_0 a \sim 2\pi n, \quad \Rightarrow \quad \omega_n = \sqrt{c^2 + (\pi n/a)^2} + O(\omega^{-1}), \quad \text{as} \quad \omega \to \infty, \quad n = 1, 2, ... \tag{30}$$

The diminishing addition in eq. (30) is, obviously, a complex value. The points ω_n calculated using this asymptotics are shown in Fig. 15 (subplot for $N = 50$) by circle marks. Their location indicates the left pass-band limits.

Since the two kinds of obstacles considered in the examples above differ by the screening properties of the related single defects, one may conclude: if for one defect $\kappa^+(\omega) \to 0$ as $\omega \to \infty$ (as in the first case $\alpha \geq \varepsilon$), then, as N increases, the presence of nearly real poles results in sharp pass peaks in the transmission characteristics of a generally closed waveguide at high frequencies. And vice versa, with large N the waveguide becomes generally open at large ω except small shrinking gap bands, if with one defect $\kappa^+(\omega) \to 1$ as $\omega \to \infty$.

It is reasonable to suppose that with increasing N the pass and stop bands become the same as for the string with an infinite periodic set of defects. In accordance with the Bloch-Floquet theory, the wave propagation eigensolution for a periodic structure is of the form
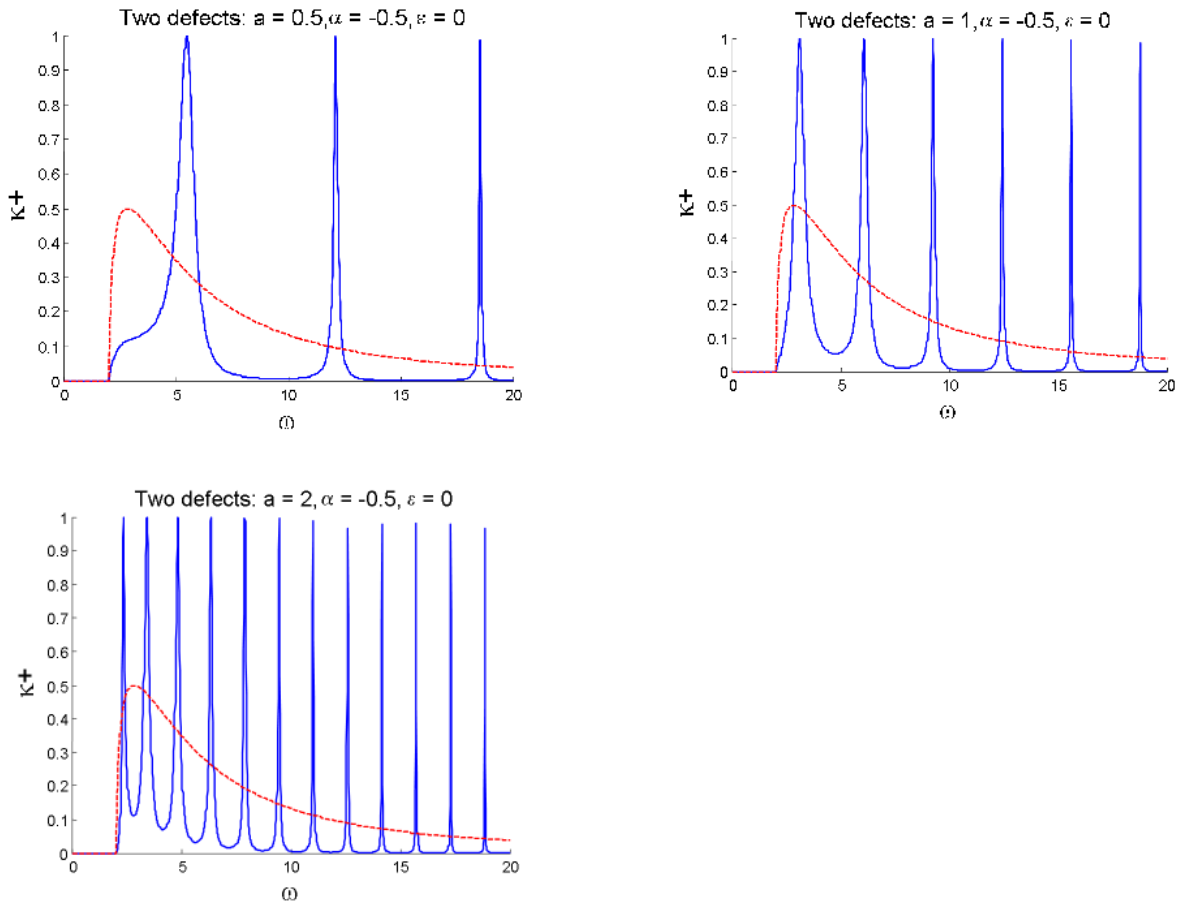
$$w(x, \omega) = e^{i\beta x} v(x, \omega) \tag{31}$$

Fig. 14 Wave transmission through two-defect zones with the spacings $a = 0.5, 1$ and 2.

where v is a periodic function: $v(x + a) = v(x)$, a is a space period of the structure, β is a wave number. The relation between β and ω is specified by a certain characteristic equation $\Delta(\beta, \omega) = 0$ following from the governing equations and boundary conditions for the periodic structure under consideration. The real roots of this equation $\omega = \omega_n(\beta)$ or $\beta = \beta_n(\omega)$ indicate the existence of propagating waves with the relative parameters ω and β, i.e. the pass bands; while the non-existence of real roots for certain frequency ranges points out the corresponding gap bands.

The Bloch-Floquet characteristic equation for the string waveguide has been derived in the form

$$\cos a\beta = \cos ak_0 + \frac{da}{k_0}\sin ak_0, \quad d = c^2\varepsilon - \omega^2\alpha. \tag{32}$$

Since $|\cos a\beta| < 1$ with real β, this equation may have real roots if and only if

$$\left|\cos ak_0 + \frac{da}{k_0}\sin ak_0\right| < 1. \tag{33}$$

In that way we have arrived at the condition controlling the existence of frequency pass bands in the periodically-defected string. At high frequencies the bounds of the pass and stop ranges may be roughly estimated by taking into account the asymptotic behavior

$$\frac{da}{k_0} \sim \begin{cases} O(\omega), & \alpha \neq 0 \\ O(\omega^{-1}), & \alpha = 0 \end{cases}, \quad \text{as} \quad \omega \to \infty.$$

With $\alpha \neq 0$ it implies

$$|\sin ak_0| \sim O(\omega^{-1}) \quad \Rightarrow \quad |ak_0 + \pi n| < \delta_n \to 0, \quad \text{as} \quad \omega \to \infty$$
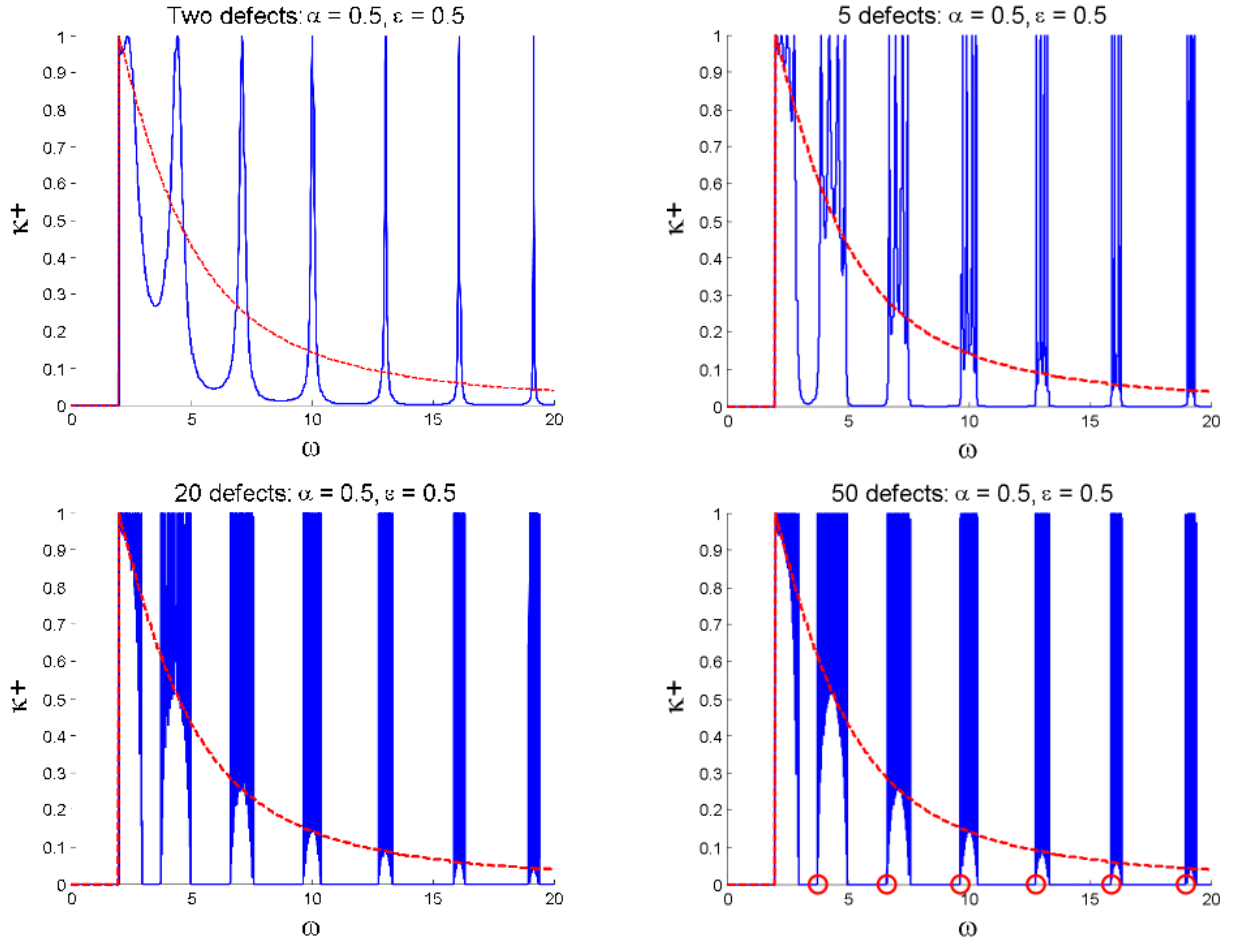
Fig. 15 Wave transmission through systems of N equally spaced ($a = 1$) combined ($\alpha = \varepsilon = 0.5$) defects for $N = 2, 5, 20$ and 50; pass bands formation with large N and their contracting into pass frequencies with large ω.

$$\text{or} \quad |\omega - \omega_n| < O(\delta_n), \quad \omega_n = \sqrt{c^2 + (\pi n/a)^2}.$$

In other words the pass bands of small width $O(\delta_n)$ shrink to the frequencies ω_n as $\omega \to \infty$. This estimation is in complete agreement with the pass band structure shown in Fig. 15 and with the two-defect estimation (30).

If $\alpha = 0$, the inequality (33) permits almost all ω except that belonging to similar small ranges (gap bands) degenerating into the stop-frequencies ω_n just as in the case of base defects shown in Fig. 16.

The numerical evaluation of inequality (33) yields just the same pass-band intervals as ones formed with increased number of obstacles in Figs. 15 and 16. It is worthy to note that the pass peaks of Fig. 15 are similar to ones for 1D resonant transmission through a finite periodic layered structure (e.g. Fig. 2 from [19]), while the pass band formation shown in Fig. 16, $N = 20$ is of qualitatively the same appearance as the transmission plots for phononic lattices presented in Figs. 5, 6 from [17].

6.3 Almost periodic obstacles

A natural question arises: how a slight disturbance of the defects' periodicity might effect on the pass and gap bands formation. The disturbance may be produced by different ways: by taking away one of defects, by inserting an extra one into a periodic group, by the distance variation between two neighbor obstacles keeping the even spacing among the others. One may also change α_j and ε_j characteristics for one of equal defects, etc. Certainly, it is hardly possible to accomplish more or less thorough analysis for all such effects at once. Figs. 17 – 22 just give some elementary examples.

First of all, based upon previous examples one may conclude that the step-intervals of transmission peaks for a set of uniformly allocated obstacles depend only on their spacing a. Hence, a variation of their properties retaining the same
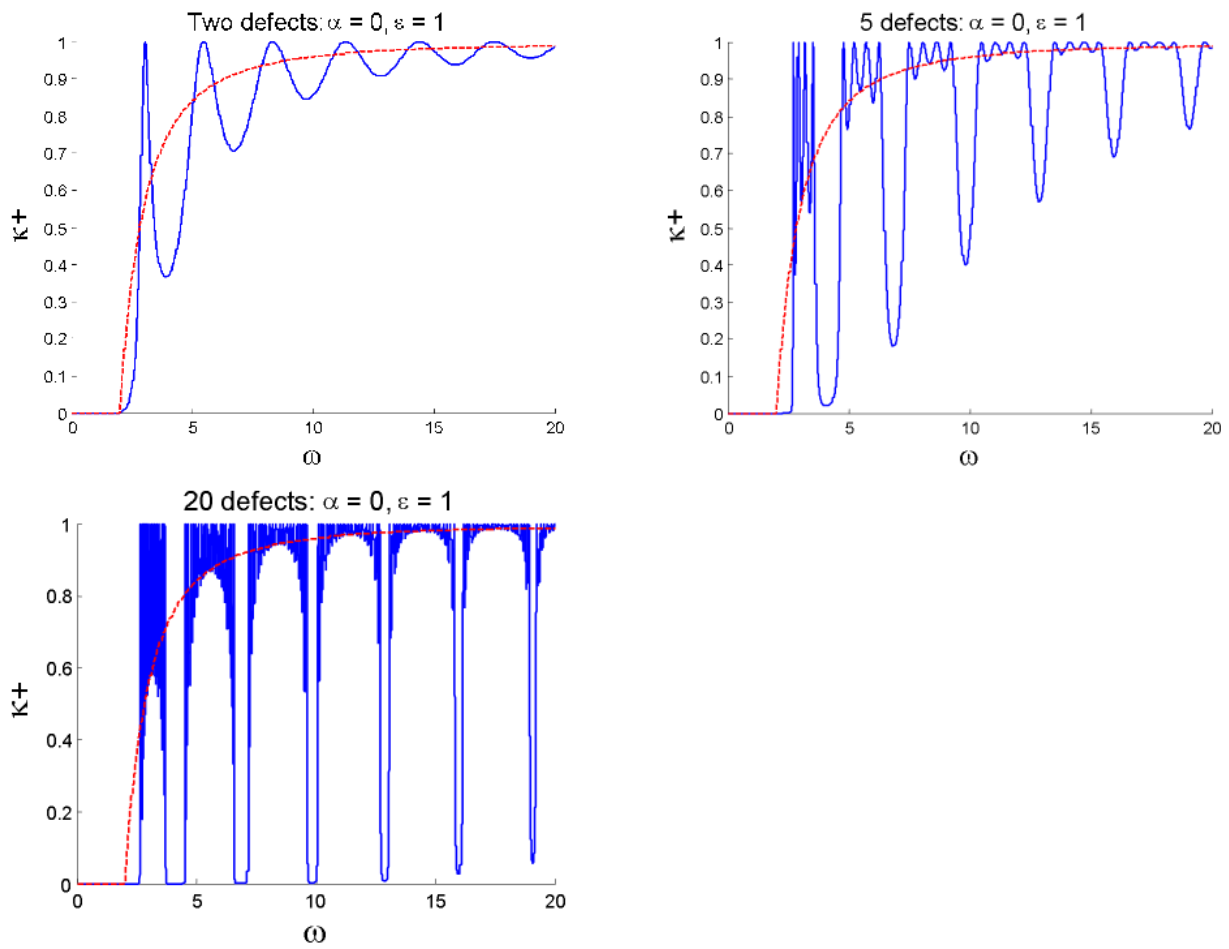
Fig. 16 The same as in Fig. 15 in the case of intact string ($\alpha = 0$) and defected elastic base ($\varepsilon = 1$); contracting gap bands.
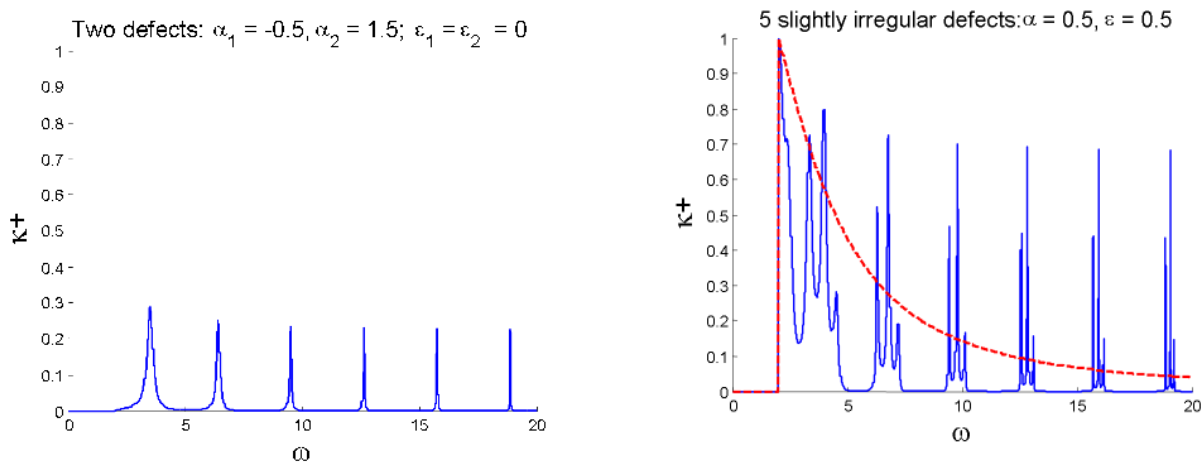

Fig. 17 Wave transmission in the case of two different string defects (compare Fig. 14).

Fig. 18 Wave transmission through 5 defects as in Fig. 15 but with the changed properties $\alpha_3 = \varepsilon_3 = -0.5$ of the middle one.
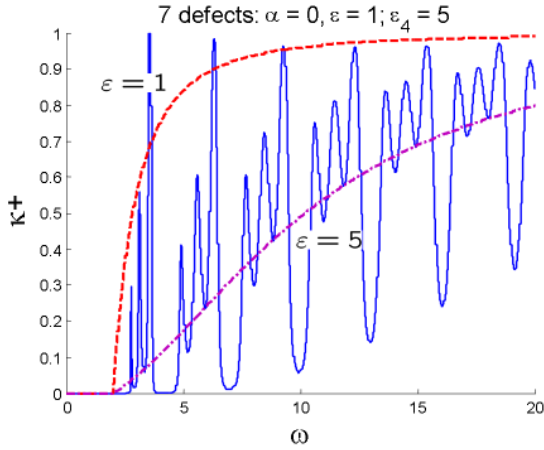
Fig. 19 Wave transmission through the periodic system of spring defects as in Fig. 16 but with the only property deviation $\varepsilon_4 = 5$.
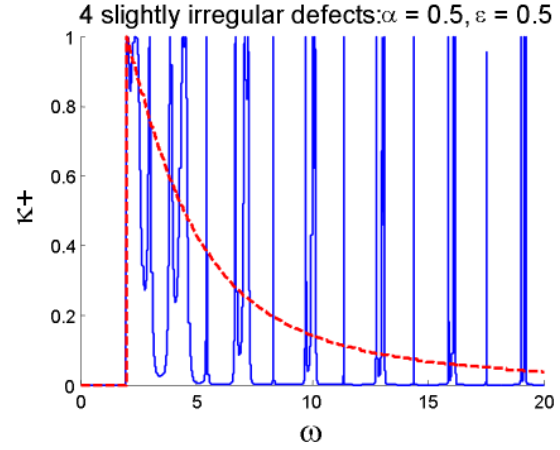
Fig. 20 Transmission through the system of defects as in Fig. 15 for $N = 5$, but with the eliminated middle one ($N = 4$, $|x_1 - x_2| = |x_3 - x_4| = 1$, $|x_2 - x_3| = 2$).
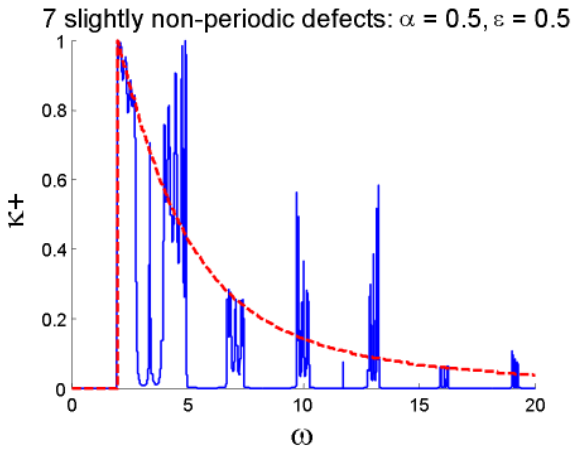

Fig. 21 Wave transmission through the quasi-periodic system of the same spring defects as in Fig. 15 with the only changed distance $|x_4 - x_5| = 0.3$.
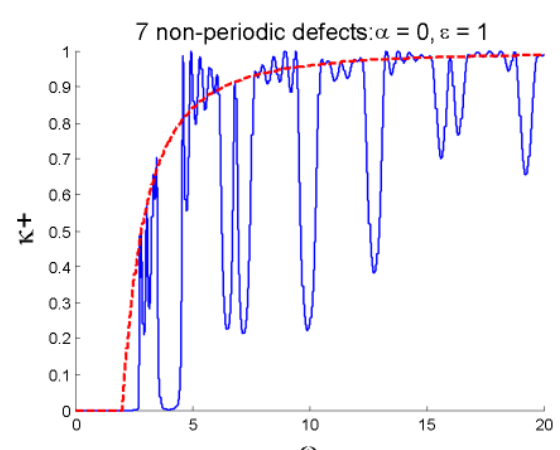

Fig. 22 The same quasi-periodicity as for Fig. 21 but for the spring defects as in Fig. 16.

location should not yield additional peaks or change the step of peak arising, although the height and shape of those peaks can be considerably transformed. For example, instead of the uniformly repetitive full-pass frequencies filtering out by two equal string defects, $\alpha_1 = \alpha_2 = -0.5$, $\varepsilon = 0$, $a = 1$ (Fig. 14), the change of the second-defect characteristics onto $\alpha_2 = 1.5$ results in no more than 30% maximal wave transmission, but at the same central frequencies (Fig. 17). Similarly, the plots of Figs. 18 - 19 for periodic defects with changed properties of the middle one demonstrate essential deformation of the peaks' shape retaining the same pass and gap bands as with the reference periodic sets given in Fig. 15 and Fig. 16, respectively.

The effect of slight distance irregularity is illustrated by Figs. 20 - 22. Since the frequency step is inversely proportional to the spacing a, the duplicate distance $|x_2 - x_3| = 2$ in the example of Fig. 20 results in additional small peaks appearing between the every two main ones. Not to mention that the poles ω_n appear under the small peak frequencies, as well. Conformably, the reduced distance $|x_4 - x_5| = 0.3$ leads to additional peaks arising with the enlarged frequency step $\Delta\omega \approx \pi/0.3$. In Fig. 21 they are visible at $\omega \approx 3$ and 12, while in Fig. 22 they are distinguishable at $\omega \approx 7$ and 16.

The results obtained are in accordance with the consideration [26] that the photonics-based devices (e.g. frequency filters) do not exhibit in real non-ideal conditions so nice properties as it was expected from the calculations for ideally periodic photonic crystals.

7 Conclusion

A semi-analytical approach to wave propagation and diffraction analysis of one-dimensional elastic waveguides with point-wise defects has been presented. It proved to be a convenient tool providing an insight into fine wave phenomena such as resonance trapped-mode, gap-band and pass-band effects and their connection with the spectral properties of a defected structure. In particular, it has been ascertained that the location of spectral points of the problem in the complex frequency plane controls the wave transmission through the defected zone. The mechanism of pass-band formation inside a wider gap-band due to the concentration of complex spectral points near the real axis at certain frequency ranges has been demonstrated. As the number of identical evenly spaced defects increases, the pass and gap bands become the same as that obtained within the Bloch-Floquet theory. It is also shown that a slight disturbance of the defect's periodicity may considerably change the stop and transmission properties.

References

[1] F. Ursell, Trapping modes in the theory of surface waves, Proc. Camb. Phyl. Soc. **47**, 347–358 (1951).
[2] D.V. Evans, C.M. Linton, Trapped modes in open channels, J. Fluid Mech. **225**, 153–175 (1991).
[3] A.K. Abramian, V.L. Andreyev, and D.A. Indeitsev, Trapped modes of oscillation in an elastic system, J. Tech. Acoust. **2**(3), 3–17 (1995).
[4] K-K Voo, Trapped electromagnetic modes in forked transmission lines, Wave Motion **45**(6), 795–803 (2008).
[5] I.I. Vorovich, Resonance properties of an elastic strip, Sov. Phys. Dokl. **24**, 304–306 (1979).
[6] Yu.I. Bobrovnitskii, M.P. Korotkov, Resonances of inhomogeneous waves in extended elastic structures, Soviet physics. Acoustics **37**(5), 453-457 (1991).
[7] V.A. Babeshko, Virusy vibroprochnosti, Izvestiya vuzov. Sev.-Kavk. region. Spets. vypusk, 90-91 (1994) (in Russian).
[8] E.V. Glushkov and N.V. Glushkova, Blocking property of energy vortices in elastic waveguides, J. Acoust. soc. Am. **102**(3), 1356–1360 (1997).
[9] E. Glushkov, N. Glushkova, M. Golub, and A. Boström, Natural resonance frequencies, wave blocking, and energy localization in an elastic halfspace and waveguide with a crack, J. Acoust. soc. Am. **119**(6), 3589–3598 (2006).
[10] A. Raghavan, C. E. S. Cesnik, Review of Guided-wave Structural Health Monitoring, The Shock and Vibration Digest **39**, 2007, 91–114 (2007).
[11] Zh. Su, Lin Ye, Ye Lu, Guided Lamb waves for identification of damage in composite structures: A review, Journal of Sound and Vibration **295**, 753–780 (2006).
[12] W.P. Mason, Physical Acoustics. Principles and methods. vol. 1, part A. (Ed. Academic Press, New York 1964).
[13] A. Figotin, Yu. A. Godin, I. Vitebsky, Two-dimensional tunable photonic crystals, Physical Review B **57**(5), 2841-2848 (1998).
[14] E.L. Ivchenko, A.N. Poddubnyi, Resonant three-dimensional photonic crystals, Physics of the Solid State **48**(3), 581–588 (2006).
[15] J.O. Vasseury et al., Experimental evidence for the existence of absolute acoustic band gaps in two-dimensional periodic composite media, J. Phys.: Condens. Matter. **10**, 6051-6064 (1998).
[16] Ch. Zhang, D. Gross, On wave propagation in elastic solids with cracks (Computational Mechanics, Publ, Southampton 1998).
[17] M. Sigalas et all, Classical vibrational modes in phononic lattices: theory and experiment, Z. Kristallogr. **220**, 765-809 (2005).
[18] A. Avila, G. Griso, B. Miara, Bandes phononiques interdites en elasticite linearisee, C. R. Acad. Sci. Paris, Ser. I., **340**, 933-938 (2005).
[19] V.Y. Zhang, J.E. Lefebvre, T. Gryba, Resonant transmission in stop bands of acoustic waves in periodic structures, Ultrasonics **44**, e899-e904 (2006).
[20] E.V. Glushkov, N.V. Glushkova, and M.V. Golub, Blocking of traveling waves and energy localization due to the elastodynamic diffraction by a crack, Acoustical Physics **52**(3), 259–269 (2006).
[21] E.V. Glushkov, N.V. Glushkova, M.V. Golub, and C. Zhang, Resonance blocking of traveling waves by a system of cracks in an elastic layer, Acoustical Physics **55**(1), 8–16 (2009).
[22] N. Glushkova, E. Glushkov, M. Golub, A. Boström, Trapped-mode and gap-band effects in elastic waveguides with obstacles, PAMM, Special Issue: 79th Annual Meeting of the International Association of Applied Mathematics and Mechanics (GAMM) (WILEY InterScience, Bremen, 2008), **8**(1), 10683-10684.
[23] E.V. Glushkov, N.V. Glushkova, M.V. Golub, and A.A. Eremin, Existence of resonant transmission zones in wide blocking range for an elastic waveguide with a system of rigid inclusions, Proceedings of the XII International Conference "Advanced Problems of Solids" (Rostov-on-Don, V. 1, 2008) 47-51 (in Russian).
[24] A.V. Vostroukhov and A.V. Metrikine, Periodically supported beam on a visco-elastic layer as a model for dynamic analysis of a high-speed railway track, Int. J. Solids Struct. **40**(21), 5723–5752 (2003).
[25] K.F. Graff, Wave motion in elastic solids (Oxford: Clarendon Press 1975).
[26] A.V. Lavrinenko, W. Wohlleben, R.J. Leyrer, Influence of imperfections on the insulating and guiding properties of finite Si-inverted opal crystals, Opt Express **17**(2), 747–760 (2009).